Validation of a BEM correction model for swept blades using experimental data

Fritz, Erik; Boorsma, Koen; Ferreira, Carlos

DOI
10.1088/1742-6596/2767/2/022035

Publication date
2024

Document Version
Final published version

Published in
Journal of Physics: Conference Series

Validation of a BEM correction model for swept blades using experimental data

Journal of Physics: Conference Series **2767** (2024) 022035 doi:10.1088/1742-6596/2767/2/022035

Validation of a BEM correction model for swept blades using experimental data

Erik Fritz[1,2], **Koen Boorsma**[1], **Carlos Ferreira**[2]

[1] Wind Energy, TNO Energy Transition, Petten, Netherlands
[2] Faculty of Aerospace Engineering, Technical University of Delft, Delft, Netherlands

E-mail: e.fritz@tno.nl

Abstract. This study validates a correction model, which extends standard blade element momentum theory to swept blades and, by doing so, enhances wind turbine simulation predictability for these advanced geometries. This correction model addresses limitations in BEM algorithms, accommodating the complexities of swept blades by considering the sweep-induced tip vortex displacement and curved bound vortex self-induction. The validation is based on previously published results from wind tunnel experiments on a horizontal axis wind turbine with straight and swept blades, providing blade-level aerodynamic data for comprehensive numerical comparisons. In both blade configurations (straight and swept), good agreement is found between experimental and numerical results, validating the numerical approach. For the swept blade case, an additional comparison to a BEM algorithm assuming a straight blade and to one accounting for crossflow is drawn, underscoring the former's inadequacy for swept blades. Comparably minor differences between the fully-corrected and only crossflow-corrected algorithms render the assessment of the proposed BEM correction model's added benefit uncertain. Using the validated BEM algorithm, the experimental results are corrected for twist deformations of individual blades, enabling a direct comparison of the campaigns with straight and swept blades. Results align with expectations, indicating sweep-induced reductions in axial induction and blade loads in the swept blade section.

1. Introduction

Wind turbine blade sweep is defined as the displacement of the blade axis in the rotor plane. This form of geometry modification has potential as a passive load alleviation mechanism [1, 2], achieved by coupling the bending and torsional deformations. Exemplary, an aft-swept blade under flapwise loading twists to lower angles of attack, thereby, reducing the aerodynamic loading.

To harvest the full potential of blade sweep, the aerodynamic properties of swept blades need to be accurately modelled by low fidelity simulation tools on which the design and optimisation processes of modern wind turbine blades rely. In recent years, research has been conducted regarding the correct numerical modelling of swept blades [3, 4, 5]. The model proposed by Fritz et al. [4] corrects blade element momentum theory (BEM) so that it can account for swept blade shapes while retaining BEM's streamtube independent approach as well as its computational efficiency. The model currently lacks experimental validation, an issue the present research aims to provide.

To this end, the data from two wind tunnel campaigns, one with straight blades [6] and one with swept blades [7], are compared to the results of the corrected BEM algorithm. The

experimental dataset consists of flow fields which are measured at the blade level of a rotating, scaled horizontal axis wind turbine (HAWT) using a stereoscopic particle image velocimetry (PIV) setup. These flow fields are postprocessed to obtain the spanwise distribution of several aerodynamic quantities, which can be directly compared against numerical simulation results.

2. Methodology

2.1. Wind tunnel experiment

Scaled wind turbine model:

A model HAWT with a rotor diameter of 1.8 m is placed in the Open Jet Facility (OJF) of TU Delft. Both wind tunnel campaigns were run with a tip speed ratio of $\lambda = 9$. The straight reference blades are 1:133 scaled versions of the IEA 15 MW reference wind turbine (RWT) blades [8], designed to match the non-dimensionalised spanwise thrust distribution of this reference. This scaling was based on conditions just below the rated wind speed of the IEA 15 MW RWT, namely at $U_\infty = 10$ m/s. While the carbon fibre composite blades were intended to be rigid to enable a purely aerodynamic analysis, non-negligible deflections occurred during the experiment as described in Section 3.1. The blade geometry is defined by the *SD7032* airfoil, which has been thoroughly characterised [9] and has been used in multiple wind tunnel models of comparable scale [10, 11]. A detailed description of the blade model development is given in [6]. The blades' chord and twist distribution are given in Figure 1.

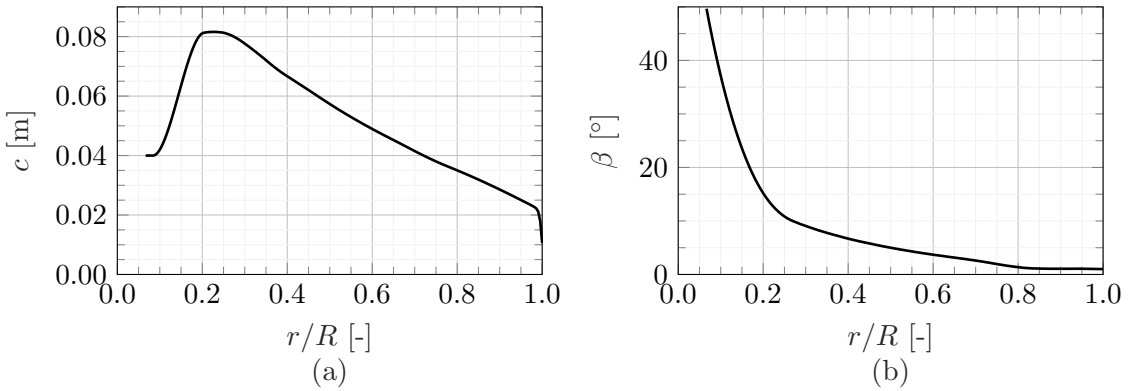

Figure 1. Chord (a) and twist (b) distribution of the scaled wind tunnel model blades

The swept blades are derived from the straight reference by gradually displacing the blade axis in the plane of rotation, starting from 50 % blade radius and with a tip displacement of 20 % blade radius. The swept planform is scaled to maintain a tip radius identical to that of the straight blade. Figure 2 shows the resulting blade axis shape.

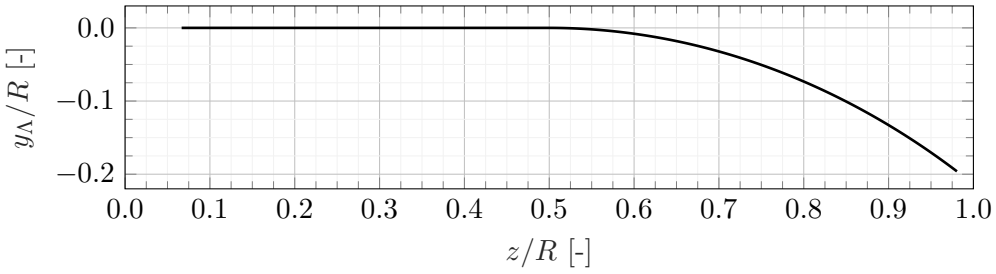

Figure 2. Swept blade axis

The used airfoil, as well as the chord and twist distribution of the swept blades, are identical to their straight reference, and the airfoils are kept perpendicular to the local blade axis in the creation of the blade geometry. A more elaborate description of the swept blades is given in [7]. Both sets of blades are shown in Figure 3 (a).

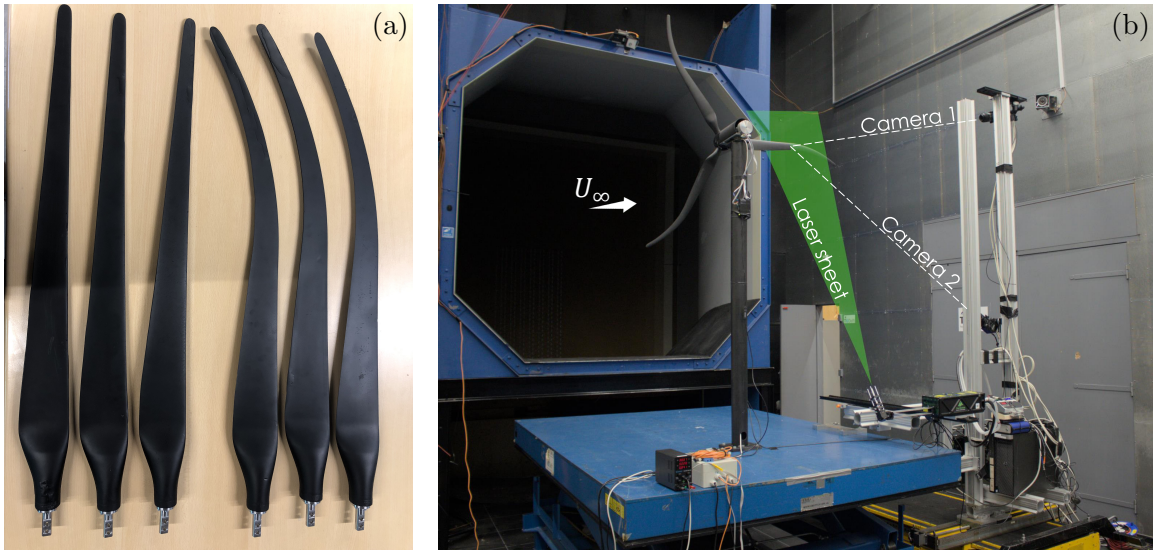

Figure 3. Straight and swept model wind turbine blades (a) and experimental setup including the PIV measurement system (b)

Measurement system:
The flow field around multiple blade cross-sections is measured using a stereoscopic PIV setup. This consists of a Quantel Evergreen double-pulsed Nd:YAG laser and a set of LaVision Imager sCMOS cameras mounted rigidly on a traversing system such that a wide range of radial locations can easily be measured without the need for recalibration. Using laser optics, a vertical laser sheet aligned with the inflow is generated. Smoke particles are used as tracers to visualise the flow. Laser and cameras are triggered through an optical sensor activated once per revolution by a notch on the turbine's main shaft, thus ensuring phase-locking. 120 phase-locked images are captured per measurement plane with the blade in the horizontal position during its upward movement. For a more detailed description of the measurement system, the reader is referred to [6]. The experimental setup is shown in Figure 3 (b) with the swept blades mounted.

Derivation of blade-level aerodynamics from PIV measurements:
The PIV-precessed velocity fields are used to locally calculate various blade-level aerodynamic quantities. To calculate the relative velocity vector at each blade section, the Ferreira-Micallef approach, as described in [12], is used. Knowing this velocity vector, induction terms, the local inflow angle and the angle of attack can be calculated. The bound circulation is derived from the line integral of the velocity field along a closed curve around the blade cross-section. Then, the Kutta-Joukowski theorem is used to estimate the blade loads based on the circulation and inflow velocity, see e.g. [13]. For a detailed description of these methods, refer to [6]. Combining the data obtained at different radial locations, spanwise distributions of these quantities are derived.

2.2. Numerical modelling

A simple BEM algorithm is implemented, following the standard equations given, e.g. by Burton et al. [14]. Prandtl's tip and root loss corrections and Glauert's correction model for highly loaded rotors are implemented. In this basic form, blade element momentum theory assumes a straight blade geometry. When sweeping a wind turbine blade, however, multiple aspects regarding the blade aerodynamics change with respect to a straight reference blade. The first aspect is commonly known as crossflow principle [15]. It states that only a part of the local inflow velocity effectively contributes to the lift and drag forces, while the spanwise flow component has a negligible influence. Most BEM-based algorithms account for this to some degree. Two further aspects of blade sweep are usually not accounted for in BEM algorithms, namely the induction of the curved bound vortex on itself and the displacement of the wake vorticity, including the dominant tip vortex. Both affect the local induced velocity and, consequently, the blade loads. Fritz et al. proposed a correction model that accounts for these effects [4]. Figure 4 gives a schematic representation of the sweep-induced changes in blade aerodynamics as discussed in this section. For a more detailed rundown of the BEM algorithm, including the equations on which the correction model is built, the reader is referred to the aforementioned reference.

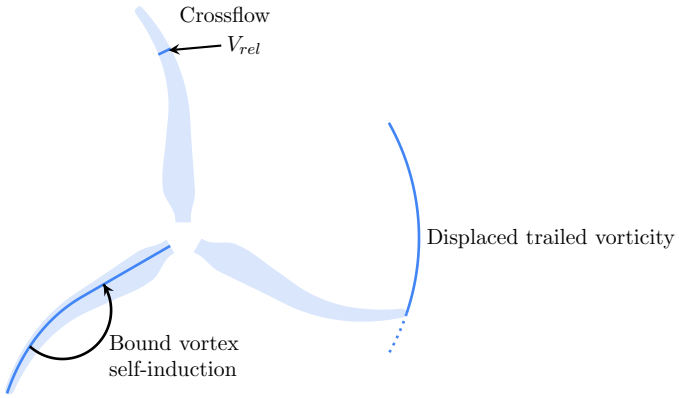

Figure 4. Schematic representation of the sweep-induced changes in blade aerodynamics

3. Results

This section presents both numerical and experimental results. The latter are presented as mean value and error bars indicating the 95 % confidence interval. This uncertainty is based on the standard deviation in the PIV-processed velocity fields. In the subsequent plots, the three blades of each wind tunnel campaign are denoted as B1, B2 and B3.

3.1. Determination of the combined pitch and twist offset

Both experimental campaigns faced the challenge of large variations in blade-level aerodynamics between the three blades. This was due to a combination of errors in the pitch angle and twist deformations, leading to varying angle of attack distributions and, consequently, different blade loading. While the pitch offset was attributed to a manually fixed pitch mechanism, the varying twist deformation was due to different stiffness properties of the vacuum-infused carbon fibre composite blades. The combined offsets in pitch/twist $\Delta\beta$ were quantified by comparing the cross-sections visible in the raw PIV images with the original blade design and applying a rotational correction until a better match was achieved. The resulting offsets to the original twist distribution are shown in Figure 5 together with quadratic curve fits that balance out unrealistic fluctuations likely due to visual misinterpretation of the images. Notable are the tip

measurements of swept blade 1, where the extremely small chord complicated the interpretation of the cross-section's orientation. Consequently, measurements with $r/R > 0.9$ were omitted in this curve fit. The curve fits are used to individually adjust each blade's twist distribution in the numerical simulations.

Originally, measurements on blades 2 and 3 were intended to demonstrate replicability. Thus, only a few selected radial positions were measured. Differences in the twist deformations were only noticed in post-processing, and additional planes could not be measured anymore.

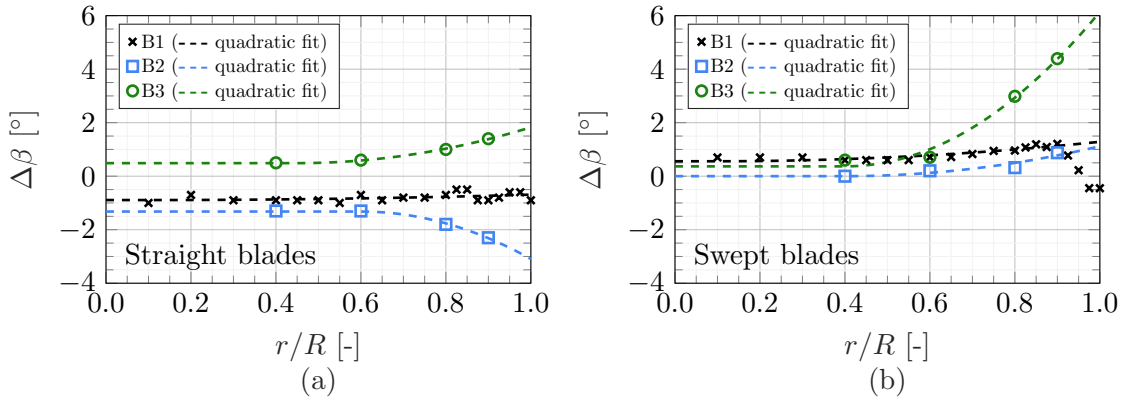

Figure 5. Combined pitch/twist offset $\Delta\beta$ from the original design twist distribution for the straight blades (a) and swept blades (b)

3.2. Validation of the straight blade simulations

The straight blade experimental campaign serves to establish a baseline regarding the agreement between BEM simulation and experimental results. Figure 6 shows the spanwise distribution of the axial induction factor a and the angle of attack α. The BEM algorithm assumes an annulus-

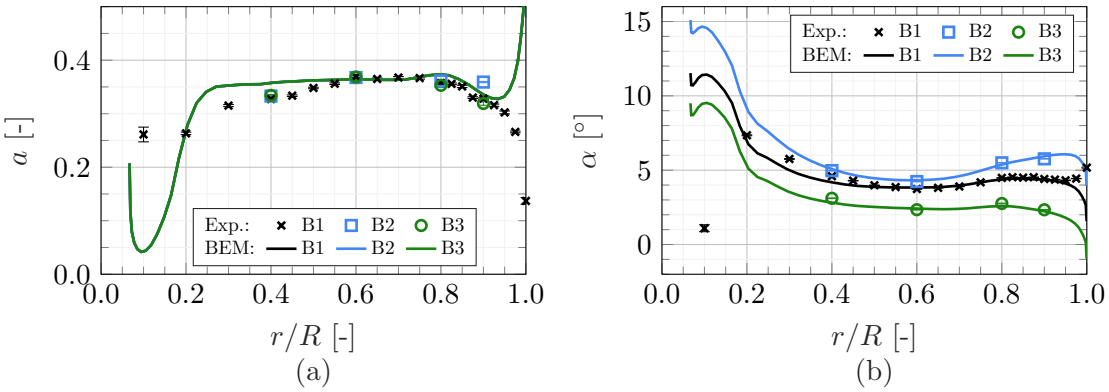

Figure 6. Spanwise distribution of the straight blades' axial induction (a) and angle of attack (b); Comparison between experiment and simulations

averaged induction factor that is a function of the sum of the three blades' axial force. Therefore, the induction factor of all three blades coincides. While arguments for the individual treatment of each blade in BEM simulations have been made [16], the experimental data exhibiting a

relatively high axial induction and operating at a high tip speed ratio justify the annulus-averaging assumption for the present case. Only at $r/R = 0.9$, where the angles of attack of blade 2 and 3 differ by 3.7°, notable differences in axial induction are present.

While there is a mismatch of induction in the inner half of the blade, simulation and experiment are well aligned in the outer half. Towards the tip, BEM predicts an increase in induction not visible in the experimental data. This is a numerical artifact of the Prandtl tip correction forcing the blade loads towards zero at the tip by decreasing the angle of attack.

With the exception of the measurement point at $r/R = 0.1$ and those closest to the tip, the angle of attack distributions of experiment and simulation match remarkably well. The discrepancies at the tip, where the experimentally derived angle of attack increases while the simulated one drops, are rooted in the application of Prandtl's tip correction, too.

The spanwise distribution of normal force F_N and tangential force F_T are given in Figure 7. Contrary to induction and angle of attack, the simulated and measured normal forces exhibit

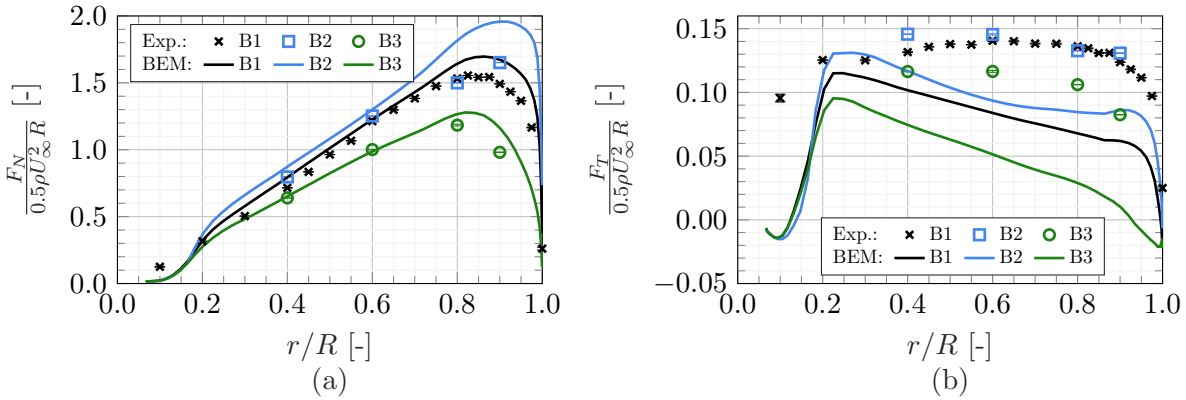

Figure 7. Spanwise distribution of the straight blades' normal (a) and tangential (b) force; Comparison between experiment and simulations

more severe discrepancies. Particularly towards the blade tip, the simulations overpredict the axial blade loading. This is also reflected in the experimental and simulated thrust coefficient $C_{T,exp} = 0.7821$ and $C_{T,sim} = 0.8563$, respectively.

There is a complete mismatch between the simulated tangential force and that derived from the PIV measurements. The experimental forces presented here are calculated using the Kutta-Joukowski theorem, which states that blade loads are linearly proportional to the bound circulation. This theorem is based on potential flow theory and, thus, neglects the viscous forces that contribute predominantly to the tangential force. In contrast to that, the BEM simulation results are obtained using viscous polars, resulting in a reduction of the tangential force. Higher angles of attack at the inboard part of the blade lead to more balance between pressure and viscous drag, which can be hypothesised to be the reason why experiment and simulation match best in this region.

3.3. Validation of the swept blade simulations

Having assessed the quality of agreement between experimental results and simulations for the straight blades, results from the BEM algorithm with sweep correction model are compared against the experimental results of the swept blade campaign. In contrast to straight blades, a distinction has to be made between loads defined per unit blade length and per unit radius for swept blades. Here, forces are presented per unit radius. During the BEM solution process,

blade element forces are calculated per unit blade length, but are corrected to unit radius when calculating the streamtube thrust coefficient [17].

Figure 8 depicts the spanwise distribution of the axial induction factor a and the angle of attack α. Compared to the straight blades case, there is a distinct drop in axial induction in the

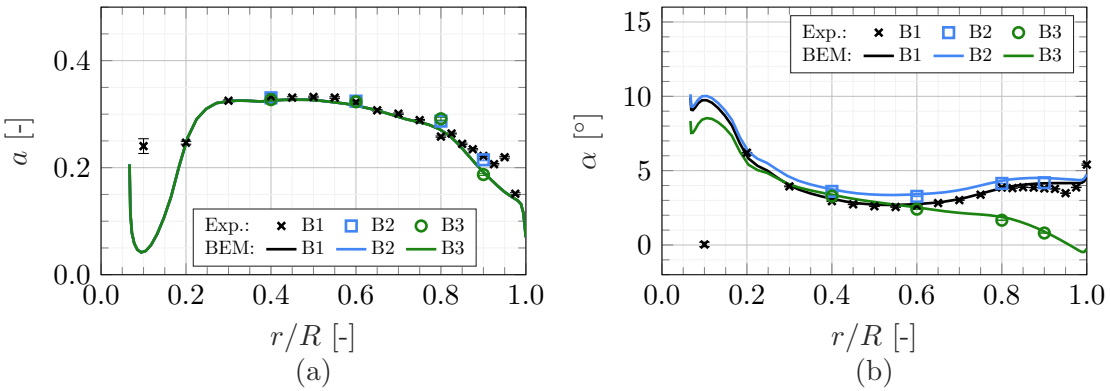

Figure 8. Spanwise distribution of the swept blades' axial induction (a) and angle of attack (b); Comparison between experiment and simulations

swept region of the blade, starting from $r/R = 0.5$. This trend is present in both numerical and experimental results. It can be attributed in part to the twist deflection towards lower angles of attack and in part to the reduced axial induction of the tip vortex, which is displaced in azimuthal direction compared to the straight reference blade. There is an excellent agreement between numerical simulations and experimental values, both regarding the axial induction and the angle of attack distribution.

With regard to the normal and tangential force, plotted in Figure 9, a pattern similar to the straight blade case can be observed. The agreement of the simulated and experimentally derived normal force is good for the inner half of the blades but worsens slightly towards the tip. Here, the simulations result in higher values than the experiment for blades 1 and 2, while the opposite is the case for blade 3. The experimentally and numerically derived thrust coefficients are $C_{T,exp} = 0.7044$ and $C_{T,sim} = 0.7121$, respectively. The tangential forces do not agree at all for reasons explained in the previous section.

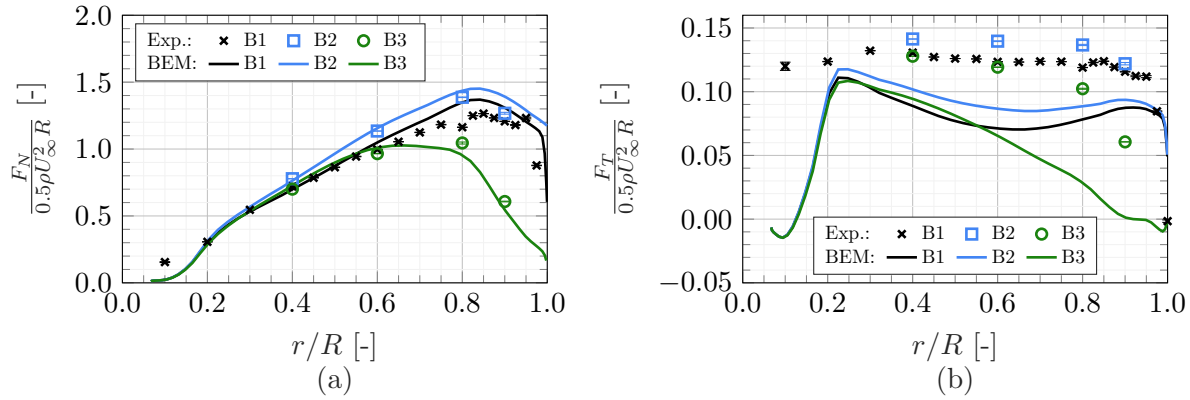

Figure 9. Spanwise distribution of the swept blades' normal (a) and tangential (b) force; Comparison between experiment and simulations

To further evaluate the benefit of the sweep correction model by Fritz et al. [4], three versions of the BEM algorithm are compared to the experimental values in Figure 10, focussing on the outer blade half where the sweep effects are present. The three versions are the BEM algorithm with sweep correction model (BEM_Λ), a version without the sweep correction model but accounting for the cross-flow principle (BEM_{cf}), and a version without any sweep related correction, essentially assuming a straight blade (BEM_0).

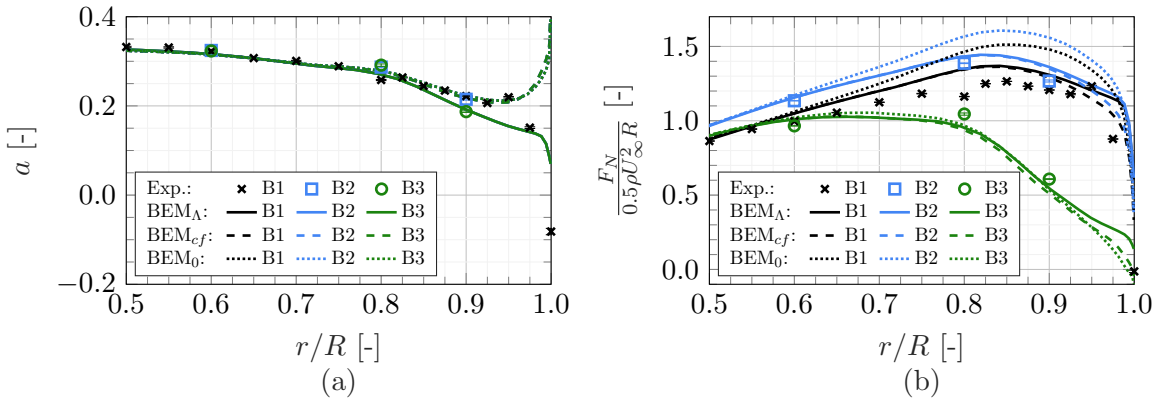

Figure 10. Comparison of various BEM implementations with the experimental results in terms of axial induction factor (a) and normal force distribution (b)

Especially from the normal force distribution, it is evident that the entirely uncorrected BEM algorithm is insufficient in simulating swept blade aerodynamics. By accounting for the misalignment of the local inflow velocity with the airfoil orientation, thus by incorporating the crossflow principle, the load reduction at the tip is captured significantly better. The added value of the BEM correction model, which accounts for the displacement of the trailed vorticity and the induction of the curved bound vorticity on itself, is more difficult to assess. By modelling the effect of the tip vortex' displacement, it enforces an additional reduction in axial induction values close to the tip. This entails an increase in angle of attack and, consequently, in the normal force distribution in this region. Given that the difference between the simulated end experimentally derived normal force distribution is larger than the difference between the crossflow-corrected and fully corrected BEM simulations, clear conclusions regarding the benefits of the BEM correction model for swept blades cannot be drawn.

3.4. Approach of correcting experimental results for pitch and twist offsets

The varying pitch offsets and twist deflections between the two measurement campaigns complicate a direct comparison of the straight and swept blade experimental results. To enable such a comparison, the BEM algorithm, validated for straight and swept blades in the previous sections, is used to approximate what the experimental results would have looked like without pitch offset and twist deflections. While the simulations presented so far used the *SD7032* airfoil polars [9] as input, these polars are now adjusted to more accurately represent the blades used in the present HAWT experiments.

Figure 11 schematically depicts this approach of adjusting the polars. The experimentally derived lift coefficient [6, 7] varies slightly from the design lift polar. For each measurement point, the original design polar is shifted until it coincides with the experimental results. The shift follows the minimal distance between polar and experimental result. This way, a new set of lift polars is defined for each measurement point of each blade while the drag and pitching moment polars are kept the same. This approach is an attempt to account for geometrical

deviations from the *SD7032* airfoil during the blade manufacturing process, which impact the local blade performance. Then, the BEM algorithm is run using these new polars but with the original design twist distribution and pitch angle. By doing so, an estimate can be made of what the experimental data would have looked like if the blades had been as rigid as intended.

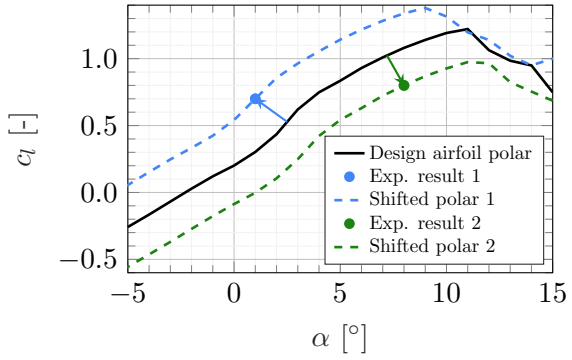

Figure 11. Schematic of the approach used to base the BEM lift polar input files on the experimentally derived lift polar

3.5. Comparison of the corrected experimental results

Figure 12 shows the spanwise distributions of axial induction factor and normal force corrected for the pitch offsets and twist deformations of each individual blade. Error bars have been omitted from these plots since there is no accurate way of knowing what the experimental uncertainties would have been in these conditions.

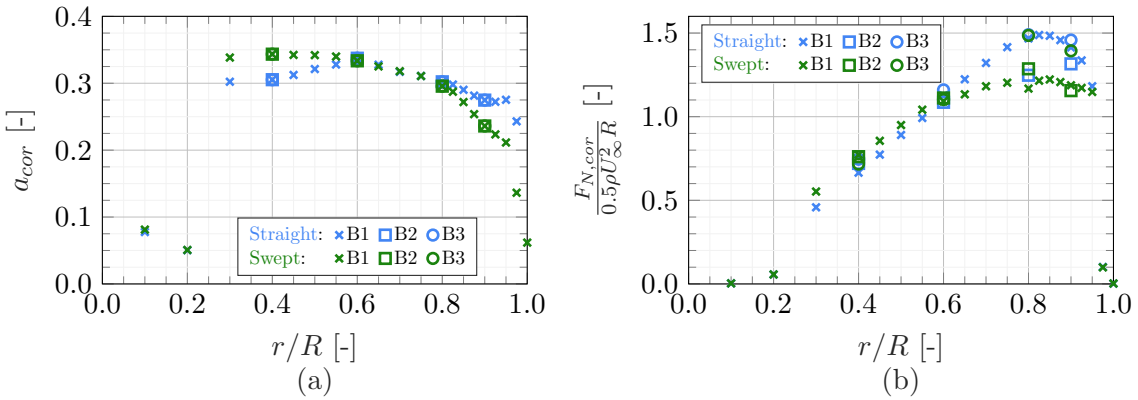

Figure 12. Comparison of corrected experimental results in terms of axial induction factor (a) and normal force distribution (b)

For $0.3 \leq r/R \leq 0.6$, where the straight and swept blade geometry are mostly identical, the swept blades exhibit higher axial induction than the straight blades. It can be speculated whether this is caused by the curved bound vortex' self-induction. Towards the blade tip, there is a drop-off in axial induction for the swept blades. This occurs due to the decreased influence of the displaced trailing wake vorticity, particularly the tip vortex. The BEM algorithm solves the momentum equation using a streamtube-average induction factor, leading to identical corrected induction values for all three blades per blade configuration. As discussed in previous sections, this is a good approximation of the conditions experienced in the experiment.

The corrected normal force distributions of the straight and swept blade, shown in Figure 12 (b), are well aligned until approximately $r/R = 0.6$. Here, the misalignment of the local inflow vector and the airfoil orientation of the swept blade leads to a reduction in lift generation and, consequently, in the airfoil's normal force. With the exception of the outer two measurement points of the swept blade 3, the corrected forces of the three blades per blade configuration are in good agreement, thereby validating the correction approach for minor deviations between design airfoil polars and experimental lift polar. The aforementioned outliers are located where the swept blade 3 experienced near-zero angles of attack, see Figure 8 (b). In this region, the *SD7032* lift curve does not follow a linear curve, which decreases the accuracy of the approach for correcting the experimental data.

From the corrected normal force distributions, the thrust coefficients can be calculated as $C_{T,cor,straight} = 0.7572$ and $C_{T,cor,swept} = 0.7362$, respectively. An overview over the thrust coefficients reported in this paper is given in Table 1. In all comparisons, the swept configuration produces less thrust than the straight one. In the straight configuration, two out of three blades twisted to higher angles of attack during the experiment. Therefore, the corrected experimental data results in a lower C_T than originally measured. In contrast to that, all swept blades twisted towards lower angles of attack. Thus, the corrected data exhibits a higher C_T than measured.

	Experiment $\beta + \Delta\beta$	BEM $\beta + \Delta\beta$	Experiment corrrected to original β
Straight	0.7821	0.8562	0.7572
Swept	0.7044	0.7121	0.7362

Table 1. Thrust coefficient C_T for various numerical and experimental configurations

4. Conclusions

This study presents an effort to validate a correction model developed to extend blade element momentum theory to swept blades. BEM-based algorithms usually assume a straight blade geometry and can account for the added complexity of a swept blade only to a certain extent. The model developed by Fritz et al. [4] aims to improve the representation of swept blades in BEM codes by accounting for the effects of an azimuthally displaced tip vortex and for the curved bound vortex' self-induction.

The BEM algorithm with sweep correction model is validated using results from wind tunnel campaigns in which a model HAWT was equipped with straight and swept blades. PIV-based flow field measurements were processed to obtain a blade-level aerodynamic description of the blades [6, 7], which can be compared against the numerical results.

To establish a baseline validation, BEM simulation results are compared against the experimental data from the campaign with straight blades. For this case, no correction model is needed, and as such, the accuracy of the basic BEM implementation can be evaluated. Overall, good agreement is found despite the fact that the three blades used in the experiment were found to have non-negligible deviations from the design twist distribution during operation.

Building on this, the BEM algorithm with sweep correction model is employed to numerically replicate the experiment with swept blade configuration. The congruence between experiment and simulation is on a comparable level as for the straight case. To assess the impact of the correction model, the swept blade experiment is also replicated with two further BEM implementations: the baseline algorithm assuming a straight blade and one which accounts for the crossflow principle. This comparison confirms that the baseline BEM implementation is insufficient to simulate the aerodynamics of the swept blades used in this experiment. Differences between the algorithm accounting for crossflow and that correcting for all sweep effects are minor,

not allowing for a clear argumentation in the sweep correction model's favour. Given that full-scale wind turbine blades would realistically be swept much less than the blades used in the wind tunnel campaigns, it could be argued that simply applying a crossflow correction in the blade element part of BEM is sufficiently accurate to model swept blade aerodynamics. The more accurate aerodynamic solution can then be coupled to a structural solver to simulate the bend-twist-coupling motivating blade sweep.

Future wind tunnel campaigns should target having blades with more consistent structural properties to avoid differences in deflection, as experienced in this study. Furthermore, the present experimental campaigns only offer data for one operating point. Future research should, therefore, aim at providing data for multiple tip speed ratios and pitch angles, so that the numerical validation can be conducted for a wider range of operating conditions. These two improvements would likely also allow a more precise evaluation of the discussed BEM correction model's impact on numerical modelling accuracy of swept blades.

Finally, the now-validated BEM algorithm is used to correct the experimental data for the experienced pitch offsets and twist deformations, enabling a direct comparison of the two experimental campaigns. Results align with expectations, showing sweep-induced reductions in axial induction and normal force in the swept part of the blade.

Acknowledgements

This contribution has been financed with Topsector Energiesubsidie from the Dutch Ministry of Economic Affairs under grant no. TEHE119018.

References

[1] Verelst D R and Larsen T J 2010 Load consequences when sweeping blades - A case study of a 5 MW pitch controlled wind turbine Tech. Rep. RISO-R-1724(EN) Technical University of Denmark, Risø National Laboratory for Sustainable Energy. Wind Energy Division, Roskilde (Denmark)
[2] Larwood S, van Dam C and Schow D 2014 *Renewable Energy* **71** 563–571 DOI 10.1016/j.renene.2014.05.050
[3] Li A, Pirrung G R, Gaunaa M, Madsen H A and Horcas S G 2021 *Wind Energy Science* **7** 129–160 DOI 10.5194/wes-2021-96
[4] Fritz E K, Ferreira C and Boorsma K 2022 *Wind Energy* **25** 1977–1994 DOI 10.1002/we.2778
[5] Horcas S G, Ramos-García N, Li A, Pirrung G and Barlas T 2023 *Wind Energy* **26** 5–22 DOI 10.1002/we.2780
[6] Fritz E, Ribeiro A, Boorsma K and Ferreira C 2024 *Wind Energy Science Discussions* Preprint DOI 10.5194/wes-2024-3
[7] Fritz E, Boorsma K and Ferreira C 2024 *Wind Energy Science Discussions* Preprint DOI 10.5194/wes-2024-11
[8] Gaertner E, Rinker J, Sethuraman L, Zahle F, Anderson B, Barter G, Abbas N, Meng F, Bortolotti P, Skrzypinski W, Scott G, Feil R, Bredmose H, Dykes K, Shields M, Allen C and Viselli A 2020 Definition of the IEA wind 15-megawatt offshore reference wind turbine Tech. Rep.
[9] Fontanella A, Bayati I, Mikkelsen R, Belloli M and Zasso A 2021 UNAFLOW: UNsteady Aerodynamics of FLOating Wind turbines URL `https://zenodo.org/record/4740006`
[10] Fontanella A, Facchinetti A, Di Carlo S and Belloli M 2022 *Wind Energy Science* **7** 1711–1729 DOI 10.5194/wes-7-1711-2022
[11] Kimball R, Robertson A, Fowler M, Mendoza N, Wright A, Goupee A, Lenfest E and Parker A 2022 *Journal of Physics: Conference Series* **2265** 022082 DOI 10.1088/1742-6596/2265/2/022082
[12] Rahimi H, Schepers J, Shen W, García N R, Schneider M, Micallef D, Ferreira C S, Jost E, Klein L and Herráez I 2018 *Renewable Energy* **125** 866–876 DOI 10.1016/j.renene.2018.03.018
[13] Anderson J D 2017 *Fundamentals of aerodynamics* sixth ed McGraw-Hill series in aeronautical and aerospace engineering (New York, NY: McGraw-Hill Education) ISBN 978-1-259-12991-9
[14] Burton T, Sharpe D, Jenkins N and Bossanyi E 2011 *Wind energy handbook 2e* (John Wiley & Sons) ISBN 0-470-69975-2
[15] Hoerner S F 1985 *Fluid-dynamic lift* (Published by Liselotte A. Hoerner)
[16] Madsen H Aa, Riziotis V, Zahle F, Hansen M, Snel H, Grasso F, Larsen T, Politis E and Rasmussen F 2012 *Wind Energy* **15** 63–81 DOI 10.1002/we.493
[17] Madsen H A, Larsen T J, Pirrung G R, Li A and Zahle F 2020 *Wind Energy Science* **5** 1–27 DOI 10.5194/wes-5-1-2020